Effect of autologous lyophilized platelet-rich fibrin on the reconstruction of osteochondral defects in rabbits

JIANWEI SUN[1*], LENG HAN[2*], CHUNDONG LIU[3*], JUNLI MA[4], XIAO LI[4], SHUOHUI SUN[4] and ZHIFA WANG[4]

[1]The Fourth Recuperate Area, Guangzhou Special Service Recuperation Center of People's Liberation Army (PLA) of China Rocket Force, Guangzhou, Guangdong 510515; [2]Department of Pathology, General Hospital of Southern Theater Command of PLA, Guangzhou, Guangdong 510010; [3]Department of Stomatology, Zhujiang Hospital, Southern Medical University, Guangzhou, Guangdong 510280; [4]Department of Stomatology, General Hospital of Southern Theater Command of PLA, Guangzhou, Guangdong 510010, P.R. China

Abstract. Osteochondral defects caused by degenerative diseases of joints, traumas and inflammation are important issues in clinical practice. Different types of autologous platelet concentrate (PCs) are used in bone and cartilage regeneration. The present study aimed to investigate the effect of lyophilized platelet-rich fibrin (L-PRF) on the repair of osteochondral defects in rabbits. L-PRF was first prepared from fresh PRF (F-PRF) through freeze-drying, and histological and microstructural observations were performed to compare the characteristics of L-PRF and F-PRF. Thereafter, these bioactive scaffolds were implanted into osteochondral defects surgically created in rabbits to assess their effects on tissue repair using micro-CT scanning, histological observations and the evaluation scoring method for cartilage repair established by the International Cartilage Repair Society (ICRS). L-PRF had a histological structure similar to F-PRF. At 16 weeks after implantation surgery, full-thickness osteochondral defects with a diameter of 5 mm and a depth of 4 mm were well-filled with newly regenerated tissues, exhibiting the simultaneous regeneration of avascular articular cartilage and well-vascularized subchondral bone, as proven through macroscopic and microscopic observations in PRF-treated groups compared with that in the untreated group. The application of L-PRF and F-PRF for osteochondral defects in rabbits contributed to massive host remodeling and reconstruction of osteochondral tissues, thus offering a prospective bioactive scaffold for the simultaneous reconstruction of articular cartilage and subchondral bone tissue.

Introduction

Most osteoarthritis (OA) resulting from degenerative diseases of joints, traumas and inflammation will unavoidably progress to osteochondral defects (1). The particular nature of hyaline articular cartilage, including the avascular nature and the low number of chondrocytes and stem cells in the surrounding cartilage lesions, results in limited potential to reconstruct osteochondral defects through a self-healing process (1,2). Moreover, to produce acceptable structural and functional repair, all three kinds of tissues involved in osteochondral lesions, including subchondral bone, the osteochondral interface and articular cartilage, need to be reconstructed simultaneously (3). Although microfractures, arthroscopic debridement, and cell-based or cell-free approaches have been introduced for osteochondral reconstruction, the clinical application and repair effects remain barely satisfactory owing to donor morbidity, possible contamination and potential problems in cell transportation (4,5). Tissue engineering and function reconstruction through host remodeling and autologous cell recruitment effectively was shown to overcome the aforementioned limitations and represent a fundamental shift from cell-based approaches (6-8).

To provide appropriate channels for the migration of recruited cells into lesion regions, marrow-stimulation techniques were applied and achieved encouraging repair results (9). Bioactive agents, including cytokines and growth factors such as stromal cell-derived factor-1, platelet-derived growth factor, VEGF, and others, were shown to promote cell recruitment and have a helpful effect on the repair of articular cartilage injuries (8,10,11). Some of the aforementioned growth factors are released from activated platelets. Consequently, different types of platelet concentrates (PCs) should also be regarded as alternative sources of autologous growth factors for cartilage regeneration (11). Platelet-rich fibrin (PRF), commonly known as a second-generation PC, was shown to have a high

Correspondence to: Professor Shuohui Sun or Professor Zhifa Wang, Department of Stomatology, General Hospital of Southern Theater Command of PLA, 111 Liuhua Road, Yuexiu, Guangzhou, Guangdong 510010, P.R. China
E-mail: gdgzsun@163.com
E-mail: kqomswang@163.com

*Contributed equally

capacity to improve wound healing and tissue repair owing to the gradual release of growth factors during its slow degradation along with its intrinsic fibrin scaffolding, which offers a unique three-dimensional (3-D) microstructure for promoting proliferation and differentiation of recruited cells (12,13). In previous studies performed by the present authors, PRF was proven to markedly promote the proliferative and osteogenic capability of bone marrow mesenchymal stem cells (BMSCs) and significantly improve the repair effect of osteogenic BMSC sheets *in vitro* and *in vivo* (14,15). Furthermore, PRF has been generally applied in oral implants, severe periodontitis, soft tissue, bone and cartilage defect repair (15). Nonetheless, fresh PRF (F-PRF) is currently difficult to apply immediately following preparation and is impossible to store for a long period and therefore impossible to commercialize (16). Several approaches for freeze-drying platelet-rich plasma (PRP) have been studied to determine storage issues and broaden its clinical application (17). Freeze-drying is a common strategy that improves the long-term preservation of these proteins and maintains their stability for tissue engineering. Lyophilized proteins in PRF not only maintain their original biological activity but also exhibit excellent stability and storage potential (18,19). The present authors previously investigated the preparation of lyophilized PRF (L-PRF) and discussed the combination of L-PRF and osteogenic BMSC sheets for bone tissue engineering in nude mice, but the repair effect of L-PRF *in vivo* remains unclear (16).

Consequently, the present study aimed to assess the potential of L-PRF in the reconstruction of osteochondral defects in rabbits using micro-CT and macroscopic and histological observations.

Materials and methods

Ethics approval. The present study was reviewed and approved by the Institutional Animal Care and Use Committee of the General Hospital of Southern Theater of PLA (Guangzhou, China; approval no. 2019010402).

Preparation of L-PRF. PRF was first prepared according to a previously published approach, with minor modifications (14). In brief, blood samples (20 ml each) were collected from the central auricular artery of rabbits and centrifuged promptly for 10 min at 1,200 x g at 26˚C in a laboratory centrifuge. These centrifuged samples were composed of three layers, with the middle layer being considered fresh PRF clot. The PRF clot was harvested with tweezers and gently pressed into a flexible, compact and elastic fibrin membrane between two sterile pieces of gauze for 10 sec to keep the membrane wet. The fresh PRF clot was referred to as F-PRF and half of the fresh clots were processed through lyophilization (freeze-drying), according to a previously published method with minor modifications (19). After freeze-drying, lyophilized platelet-rich fibrin (L-PRF) samples were obtained and stored at room temperature for 2 weeks. F-PRF should be used immediately after preparation and cannot be stored for a long period. Therefore, after L-PRF was prepared for further experiments, F-PRF was immediately prepared and used for *in vitro* and *in vivo* experiments. The prepared L-PRF and F-PRF fragments were processed for histological observation

and inspection under scanning electron microscopy (SEM; S-4800, Hitachi, Ltd.). Finally, the harvested F-PRF and L-PRF samples were preserved in sterile Petri dishes for subsequent experiments.

To acquire BMSCs, a total of 3 male 4-week-old New Zealand rabbits were euthanized by intraperitoneal injection of an overdose of barbital sodium (3%; 150 mg/kg). Briefly, limb long bone and iliac bone were dissected from the rabbits and rinsed with PBS. Subsequently, the bone marrow in the limb long and iliac bones was flushed out with DMEM-F12; (HyClone; Cytiva) supplemented with 10% FBS (HyClone; Cytiva), 200 U/ml penicillin, 100 μg/ml streptomycin and 272 μg/ml L-glutamine (all Amresco, LLC). The obtained clumps of bone marrow cells were repeatedly pipetted and dispersed to obtain a homogeneous cell suspension. Subsequently, the isolated cell suspension was plated in a 10-cm culture dish at a concentration of $5x10^5$ cells/cm^2. After the third, fifth and seventh days of seeding, floating cells were removed and fresh medium was added to the remaining adherent cells, which were considered BMSCs. The medium was changed every 3 days until the cells reached 90-95% confluence; then were subcultured at a ratio of 1:3. Second-passage BMSCs were used for experiments. Surface marker expression of BMSCs was investigated using flow cytometry (FACSCalibur™; BD Biosciences). Cells were labeled with monoclonal antibodies against CD29 (cat. no. ab95623) and CD31 (cat. no. ab24590) (all from Abcam). Differentiation into osteogenic and adipogenic lineages was also evaluated by Alizarin red staining and Oil-Red-O staining *in vitro*. Second-passage cells were obtained, cultured in osteogenic induction medium (containing 10% FBS, 10 mmol/l β-sodium glycerophosphate, 10^{-7} mol/l dexamethasone, 50 mg/l L-ascorbic acid) (all Amresco, LLC) and in adipogenic induction medium [containing 10% FBS, 1 μmol/l dexamethasone, 10 μmol/l insulin, 200 μmol/l indomethacin and 0.5 mmol/l isobutylmethylxanthine (IBMX)], respectively. Then, alizarin red staining for 8 min at room temperature and Oil-Red-O staining for 10 min at room temperature, observed and photographed under an inverted microscope (X100 and X200 of magnification, OlympasIX71).

Animal surgery. In the present study, fifteen male mature New Zealand white rabbits (age, 3-month-old; weight, 2.0-2.5 kg; Huadu Xinhua experimental animal farm, Guangzhou, China, were used. General anesthesia was induced before surgery through intravenous injection of ketamine hydrochloride (60 mg/kg) and xylazine (6 mg/kg) (7). Subsequently, the knee joint capsule was exposed sufficiently after the lateral parapatellar skin was incised. A steel trephine bar (5 mm in diameter and 6 mm in height (Taobao), which is currently applied in oral dental implant surgery, was used to produce a full-thickness osteochondral defect 5 mm in diameter and 4 mm in depth in the center of the trochlear grove. To minimize any possible variance in the operation, the same well-trained surgeon completed all the surgeries. The 24 osteochondral defects produced in 12 rabbits were randomly divided into the following three groups: i) Defects without treatment, i.e. untreated group used as a blank control; ii) defects filled with F-PRF fragments, i.e. F-PRF group; and iii) defects filled with L-PRF fragments, i.e. L-PRF group.

Finally, eight osteochondral samples in each group were subject to histological analysis.

The PRFs were cut into small pieces (~1 mm^3) and implanted into the osteochondral defects in rabbits, according to a previously published method with minor modifications (20). A total of one PRF membrane obtained from a 10 ml blood sample was used to fill one osteochondral defect. Finally, the remaining three rabbits were also surgically treated, but no osteochondral defect was created, to be used as positive control. Postoperatively, all of the rabbits were returned to their housing when they could lie on their stomachs and were conscious. Thereafter, rabbits were maintained in separate cages and allowed to move freely immediately after surgery. The vital signs of the animal were observed for the whole animal experiments process that lasted for 16 weeks; vital signs included the healing of the wound, the mental state of the rabbit, feeding and drinking conditions, the body temperature and movement. The rabbits were monitored by the present authors every day for 2 weeks after surgery and at least once every two days after the surgical area healed. Moreover, the staff of the Laboratory Animal Center monitored the rabbits every day. Furthermore, no rabbits showed treatment-specific effusions or any overt evidence of infection and all wounds healed well. After 16 weeks, all 15 rabbits were euthanized by intravenous injection of an overdose of barbital sodium (3%; 150 mg/kg) and osteochondral specimens were harvested for macroscopic assessment, micro-CT scanning and histological observations.

Gross morphology. To evaluate the effect of PRF fragments on the repair of osteochondral defects *in vivo*, the macroscopic evaluation scoring method for cartilage repair established by the International Cartilage Repair Society (ICRS), which divided four grades: Grade I: normal(12); Grade II: nearly normal (11-8); Grade III: abnormal(7-4) and Grade IV: severely abnormal (3-1), was used to examine and score specimens. At the same time, blinded scoring was calculated three times to reduce the bias as much as possible (21).

Micro-CT scanning. Micro-CT scanning and examinations (Siemens AG; 80 kV, 500 mA, 1200 msec integration time) were used to analyze the grade of repair of the articular cartilage and subchondral bone in the PRF transplanted defect areas. Briefly, the specimens were collected and fixed in 4% formaldehyde at 26˚C for 24 h and then subjected to micro-CT scanning. In addition, all of the scanning data were reconstructed in 3-D based on Cobra software (Siemens reconstruction software; version VC40) to display the newly formed bone and cartilage tissues. Furthermore, the newly regenerated bone tissue in defects was also examined and reported as the bone volume (BV)/total volume (TV) ratio to quantitatively present newly formed bone tissue in the three experimental groups. Moreover, the specimens from the three positive control rabbits were examined and reconstructed to provide reference data.

Histological and immunohistochemical examination. After macroscopic assessment and micro-CT scanning observations, 10% EDTA was used to decalcify all the collected specimens for 14 days, followed by dehydration with graded ethanol. Next, the processed specimens were embedded in paraffin, sectioned into slices of 5 μm thickness and stained with safranin-O for 3 min at room temperature to study the glycosaminoglycan distribution, stained with H&E and Masson's trichrome (MTC) for 15 min at room temperature for general histological observations, and stained with Sirius Red for 8 min at room temperature to analyze kinds of collagen in newly formed tissue. Moreover, blinded scoring based on the ICRS scale for histological evaluation was calculated three times to reduce the bias (22).

Furthermore, the expression of collagen type I (COL-I) and type II (COL-II) was investigated through immunohistochemical staining to analyze the collagen distribution in the reconstructed tissue. Briefly, sections (thickness 5 μm were blocked with 1% bovine serum albumin Gibco; Thermo Fisher Scientific, Inc.) at 37˚C for 40 min, followed by incubation with primary anti-COL-I (1:100, bs-10423R, Bioss) and anti-COL-II antibodies (1:100, bs-10589R, Bioss, Beijing, China) at 4˚C overnight. Subsequently, the secondary antibody goat anti-rabbit IgG (H+L) HRP (1:200, Cat# S0001, Affinity Biosciences, Beijing, China) was added and cultured at 37˚C for 60 min after rinsing with PBS three times. Finally, peroxidase-antiperoxidase method (PAP) and hematoxylin (for 50 sec at room temperature) was used to stain these sections for further observations. In addition, the percentage of the positive surface area occupied by COL-I and COL-II relative to the total target area (mean density=IOD Sum/Area Sum) was quantitatively calculated based on Image-Pro Plus 6.0 software (Media Cybernetics, Inc.). The signal density of tissue areas from five randomly selected fields was counted blindly and subject to statistical analysis.

Statistical analysis. SPSS version 21.0 (IBM Corp.) was used to perform the statistical analysis. Data are presented as the mean ± standard deviation. One-way ANOVA was used for multiple group comparisons, followed by Tukey's honestly significant difference tests. $P<0.05$ was considered to indicate a statistically significant difference.

Results

Characterization of L-PRF. Blood samples were separated into three layers by centrifugation with acellular plasma at the faint yellow liquid top layer (Fig. 1A-a), fibrin clots at the pale yellow gel middle layer (Fig. 1A-b) and red blood cells at the loose red jelly bottom layer (Fig. 1A-c). After the acellular plasma was removed, PRF clots were obtained easily with sterile tweezers and the red blood cells were discarded (Fig. 1B). When the fluids within the PRF matrix were gently squeezed out, a flexible, compact and highly elastic fibrin membrane was obtained, which was regarded as F-PRF (Fig. 1C). L-PRF with a loose structure and rough surface was harvested after F-PRF was freeze-dried (Fig. 1D).

H&E staining results showed that F-PRF was composed of a mass of red-stained and closely arranged fiber bundles, in which blue-stained mononuclear leukocytes were observed (Fig. 1E). In comparison, the fibrous fibrin mesh of L-PRF was not compactly aligned with abundant pores of unequal size and blue-stained mononuclear leukocytes were also observed (Fig. 1H). Microstructural examination through SEM revealed that the fibrous fibrin network was arranged more regularly
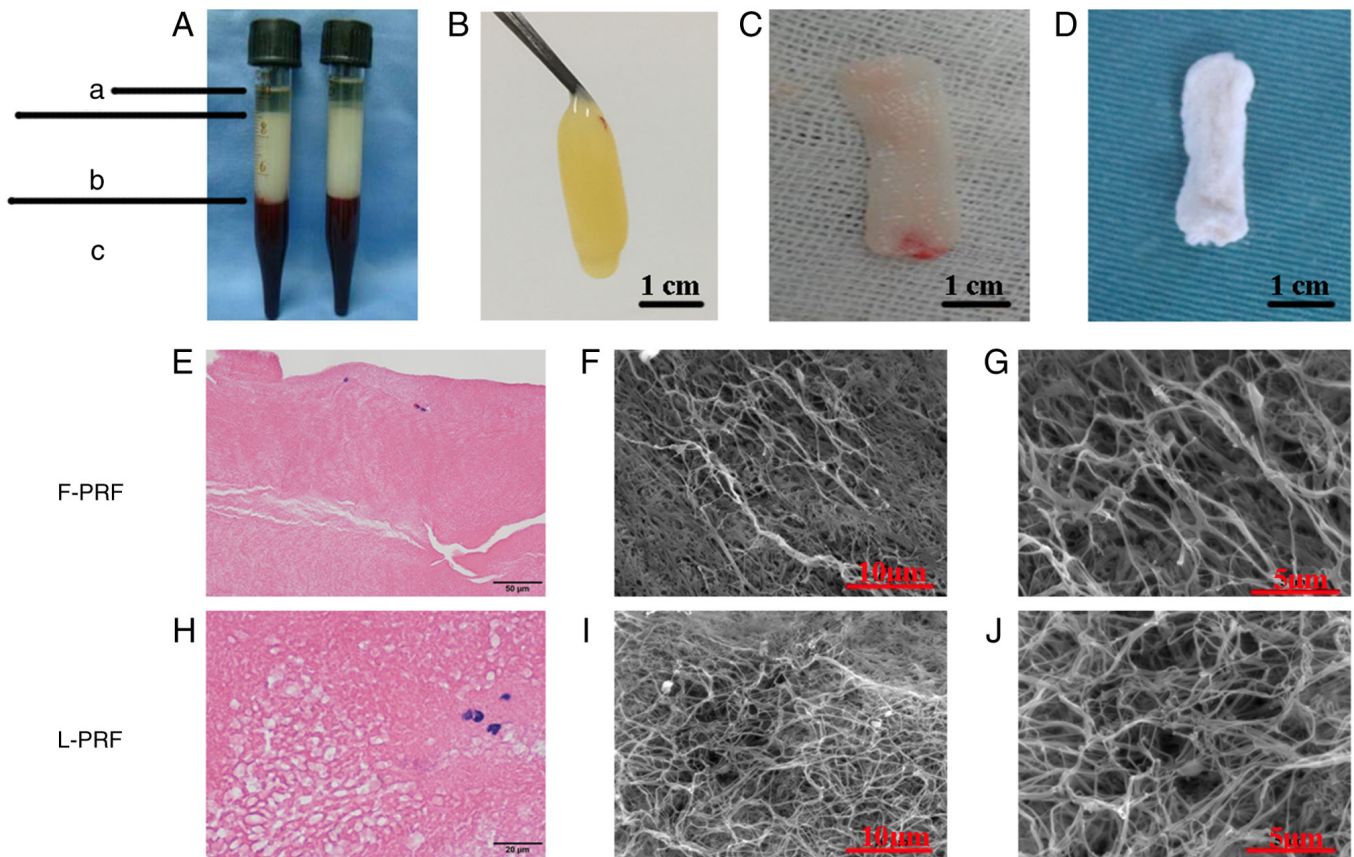
Figure 1. Characterization of L-PRF. (A) Blood samples separated into three layers through centrifugation: (A-a) Top layer is composed of acellular plasma, (A-b) The yellow gel in the middle is fibrin clots and (A-c) The bottom layer is composed of red blood cells. (B) Representative images of (B) a PRF clot, (C) a flexible, compact and elastic fibrin membrane, which was regarded as fresh PRF (F-PRF) and (D) a lyophilized L-PRF. (E) H&E staining showed that F-PRF consisted of a great number of red-stained and closely arranged fiber bundles. (F) SEM examination showed that fibrin was arranged regularly in the F-PRF. (G) High-magnification SEM images showed the three-dimensional network of F-PRF. (H) H&E staining showed that the fibrin network of L-PRF was loosely arranged. (I) SEM examination showed that the arrangement of fibrin in the L-PRF was more disordered. (J) High-magnification SEM images showed the three-dimensional network of l-PRF, which consisted of a large number of trimolecular branch junctions. PRF, platelet-rich fibrin; L-PRF, lyophilized PRF; F-PRF, free PRF.

and compactly in the F-PRF clots (Fig. 1F) than in the L-PRF (Fig. 1I). However, a large number of fibrin fibers assembled into a porous 3-D fibrin network of trimolecular branch junctions could be seen throughout both the L-PRF (Fig. 1J) and F-PRF (Fig. 1G). These histological and microstructural results indicated that freeze-drying had little effect on the 3-D microstructure of PRF.

BMSCs presented a fibroblast-like morphology and closely spaced growth (Fig. S1A) and exhibited the typical characteristics of stem cells, including rapid proliferation and self-renewal (Fig. S1B). Alizarin red (Fig. S1C) and Oil red O (Fig. S1D) confirmed their osteogenesis and adipogenesis. Moreover, the cells were highly CD29-positive (Fig. S1E) and CD31 negative (Fig. S1F), which confirmed the identification of mesenchymal stem cells.

Scheme of the knee joint osteochondral defect model in vivo. As shown in Fig. 2A, 24 defects obtained from 12 rabbits were randomly divided into three groups. In addition, the remaining three rabbits, which were only surgically skin-incised without undergoing any procedure to create osteochondral defects, were used as a normal control. The specific grouping diagram is displayed in Fig. 2B-E. After

the patella was medially dislocated, the articular joint was exposed (Fig. 2F) and a graduated stainless steel trephine bar (red arrow; Fig. 2G) was used to create an osteochondral defect, which measured 5 mm in diameter and 4 mm in depth (Fig. 2H). Fresh blood promptly occupied the defect site. Fig. 2I and J show the implantation of F-PRF fragments (black arrow) and L-PRF fragments (yellow arrow) into the defects, respectively. After the PRF fragments were placed into the defect site, they were promptly mixed with blood. Subsequently, the transplanted PRF scaffolds were pressed softly for 2 min and PRF scaffolds immersed in blood from the bone marrow cavity filled the defects (yellow arrow; Fig. 2I and J).

Macroscopic evaluations. At 16 weeks after surgery, macroscopic evaluations of the osteochondral defects showed that the newly formed tissues had a rough surface and manifested as fibrous tissues covered with a spot of cartilage-like tissue (Fig. 3A). The newly formed tissues in the L-PRF and F-PRF groups appeared fully connected with the circumambient native articular cartilage and smooth hyaline cartilage similar to that of the positive control was located on the surface (Fig. 3B-D). Furthermore, Fig. 3M showed that the
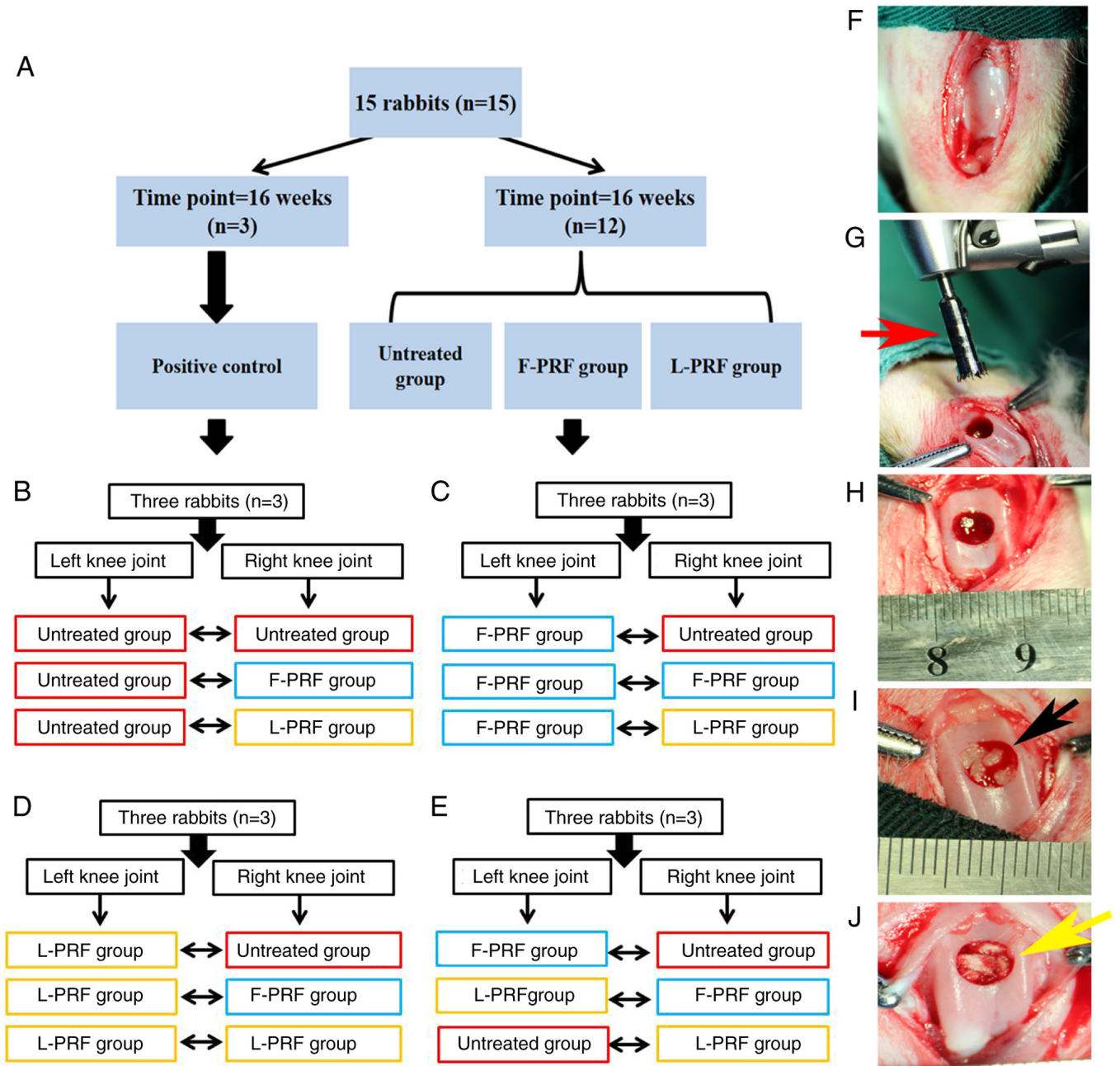
Figure 2. Animal surgery of the knee joint of rabbits. (A) Grouping scheme. (B) Left side was untreated, whereas the contralateral osteochondral defect received untreated, F-PRF, and L-PRF, respectively. (C) Left side was F-PRF, whereas the contralateral osteochondral defect received untreated, F-PRF, and L-PRF, respectively. (D) Left side was L-PRF, whereas the contralateral osteochondral defect received untreated, F-PRF, and L-PRF, respectively. (E) Left side was F-PRF, and L-PRF, and untreated, whereas the contralateral osteochondral defect received the untreated, F-PRF, and L-PRF, respectively. (F) Representative photography of an exposed knee joint. (G) Graduated stainless steel trephine bar used in creating defects (red arrow). (H) Representative photography of surgically induced cylindrical osteochondral defect with a diameter of 5 mm and a depth of 4 mm. Blood from the subchondral bone marrow cavity occupied the defect sites. (I) The complex of the F-PRF scaffold (black arrow) and blood clots adequately occupied the defect after coagulation. (J) Complex of the L-PRF (yellow arrow) scaffold and blood clots adequately occupied the defect after coagulation. PRF, platelet-rich fibrin; L-PRF, lyophilized PRF; F-PRF, free PRF.

macroscopic examination based on the ICRS scoring system provided the following mean scores for the three experimental groups: F-PRF group (10±1) showed no significant difference compared with that of the L-PRF group (9±1), which suggested that similar repair results were observed in both PRF-treated groups. The score of the untreated group (4±1) was the lowest among the three groups (P<0.05), reflecting the worst results compared with those of the PRF-treated groups.

BV/TV ratio was evaluated based on micro-CT data to analyze the newly regenerated bone tissue in the transplanted sites (Fig. 3E-L). Fig. 3E-G display the different quantities of newly regenerated bone and bone-like tissues in the different groups. The knee joints of the PRF-treated groups (Fig. 3E and G) were similar to the knee joints of the positive control (Fig. 3H). Furthermore, the newly formed bone tissues in each group showed large differences in the cross-sectional images of defect sites (Fig. 3I-L). The quantity and quality of
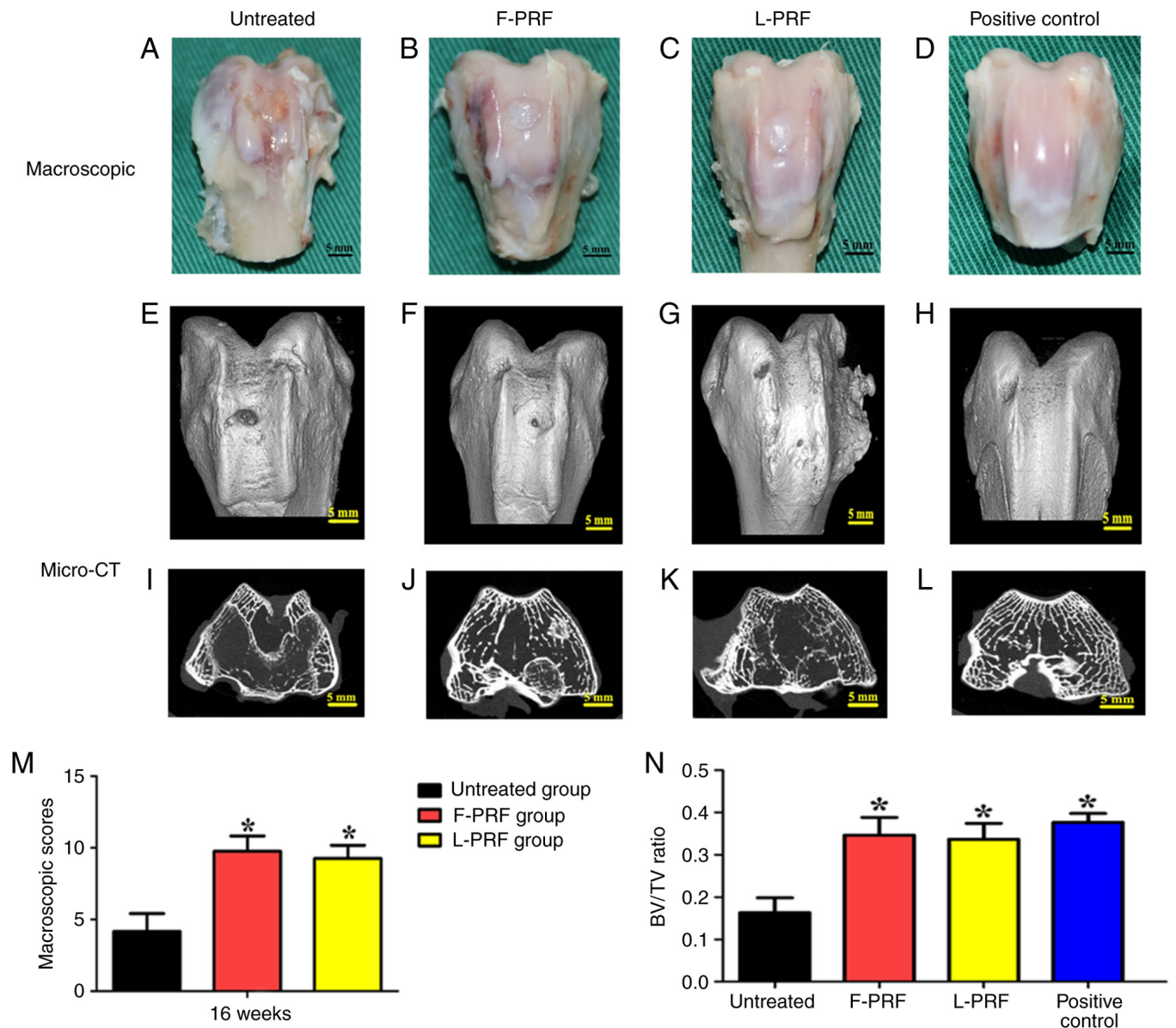
Figure 3. Macroscopic observations and micro-CT evaluation *in vivo* at 16 weeks postoperatively. Macroscopic views of the defects of the knee left (A) Untreated or reconstructed with (B) F-PRF or (C) L-PRF scaffolds. (D) Normal knee joint of rabbits (positive control). (E-H) Micro-CT 3D views of newly formed tissues. (I-L) The cross-sectional views of micro-CT displayed that the newly formed bone was different in each group. (M) Macroscopic scores of the reconstructed joint. (N) Comparison of subchondral bone regeneration based on the ratio of BV/TV (n=8). *P<0.05 vs. untreated group. PRF, platelet-rich fibrin; L-PRF, lyophilized PRF; F-PRF, free PRF.

bone tissue (BV/TV ratio) in the untreated group was significantly worse than that in the PRF-treated and normal control groups (Fig. 3N; P<0.05). Moreover, there was no obvious discrepancy between the PRF groups and the normal control group (P>0.05).

Histological examinations. Histological analysis through safranin-O, H&E, MTC and Sirius red stain and immunostaining (COL-I and COL-II) showed differences in the tissues occupying the defects in all groups at 4 months after surgery (Figs. 4 and 5). Almost no newly formed cartilage or cartilage-like tissues were observed, where the defects were filled with fibrous tissues and a small amount of cartilage tissue, and almost no hyaline cartilage formed in the untreated group (Fig. 4A). In contrast, the merged images of

safranin-O staining showed that well-regenerated cartilage and bone tissues filled the defects in the PRF-treated groups (Fig. 4B and C) and completely reconstructed the consistency of the trochlear grove surfaces of joints. In detail, in the untreated group, fibrous tissues with poor vascularization adhered to the surrounding normal tissues (Fig. 4a1-a3). By contrast, the regenerated cartilage layer in the PRF-treated groups conformed to the surrounding normal cartilage layer. Reassuringly, the characteristic hierarchical zonal cell alignments in cartilage appeared in the PRF-treated groups (Fig. 4b2 and b2), which was in accordance with the structure of normal cartilage tissue (Fig. S2C). In addition, histological staining, such as H&E and MTC, indicated well-vascularized reconstructed bone combined with newly formed cartilage (Fig. 4b2, c2, b3 and c3). The ICRS scoring method was applied
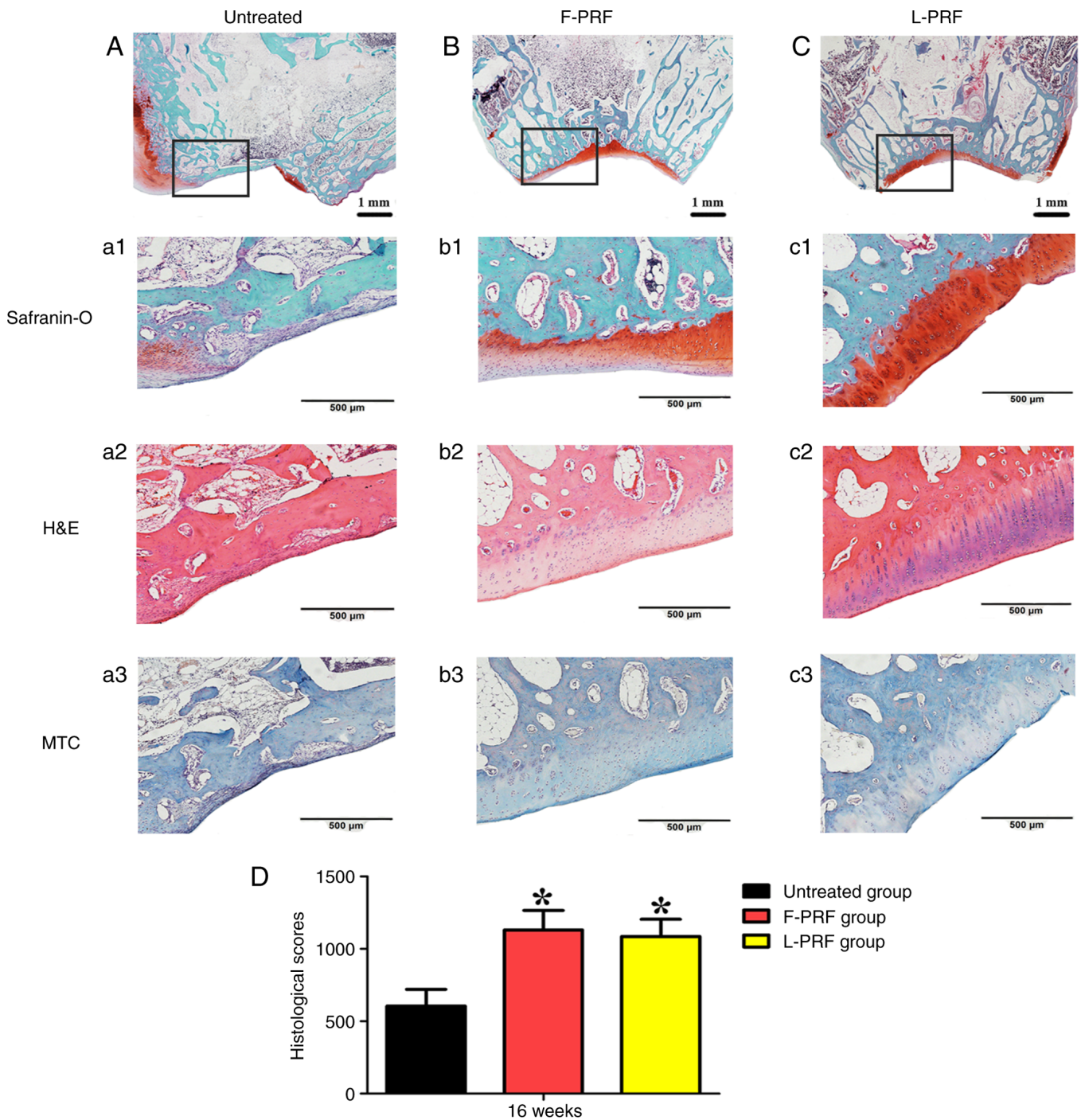
Figure 4. Histological observations at 16 weeks postoperatively. (A-C) Merged pictures of safranin-O staining. (A1-C1) Higher-magnification views showed the boundary area between repaired and native tissues in different groups. (A2-C2) H&E staining. (A3-C3) Masson's trichrome staining. (D) Histological evaluation based on the International Cartilage Repair Society scoring system. *P<0.05 vs. untreated group. PRF, platelet-rich fibrin; L-PRF, lyophilized PRF; F-PRF, free PRF.

to quantitatively analyze histological observations. The scores were 605±115 in the untreated group, 1,130±135 in the F-PRF group, and 1,085±118 in the L-PRF group at 16 weeks after surgery (Fig. 4D). The untreated group had lower scores than the PRF-treated groups (P<0.05). However, the scores in the F-PRF and L-PRF groups were similar (P>0.05).

Furthermore, the different kinds of newly formed collagen in all three groups were displayed more clearly using Sirius red staining. A large mass of regenerated cartilage matrix (blue arrow) and bone matrix (black arrow) was observed

in the PRF-treated groups (Fig. 5B and C), which was very similar to the normal cartilage in the positive control (Fig. S2D). However, in the untreated group, only a small amount of newly regenerated cartilage matrix was observed (blue arrow; Fig. 5A). Immunohistochemical COL-I and COL-II staining also indicated the phenotypic stability of the newly formed cartilage tissues in PRF-treated groups. In detail, COL-I, as a characteristic bone constituent, was weakly stained (Fig. 5E and F), whereas COL-II, as a characteristic cartilage component, was highly positively stained in the
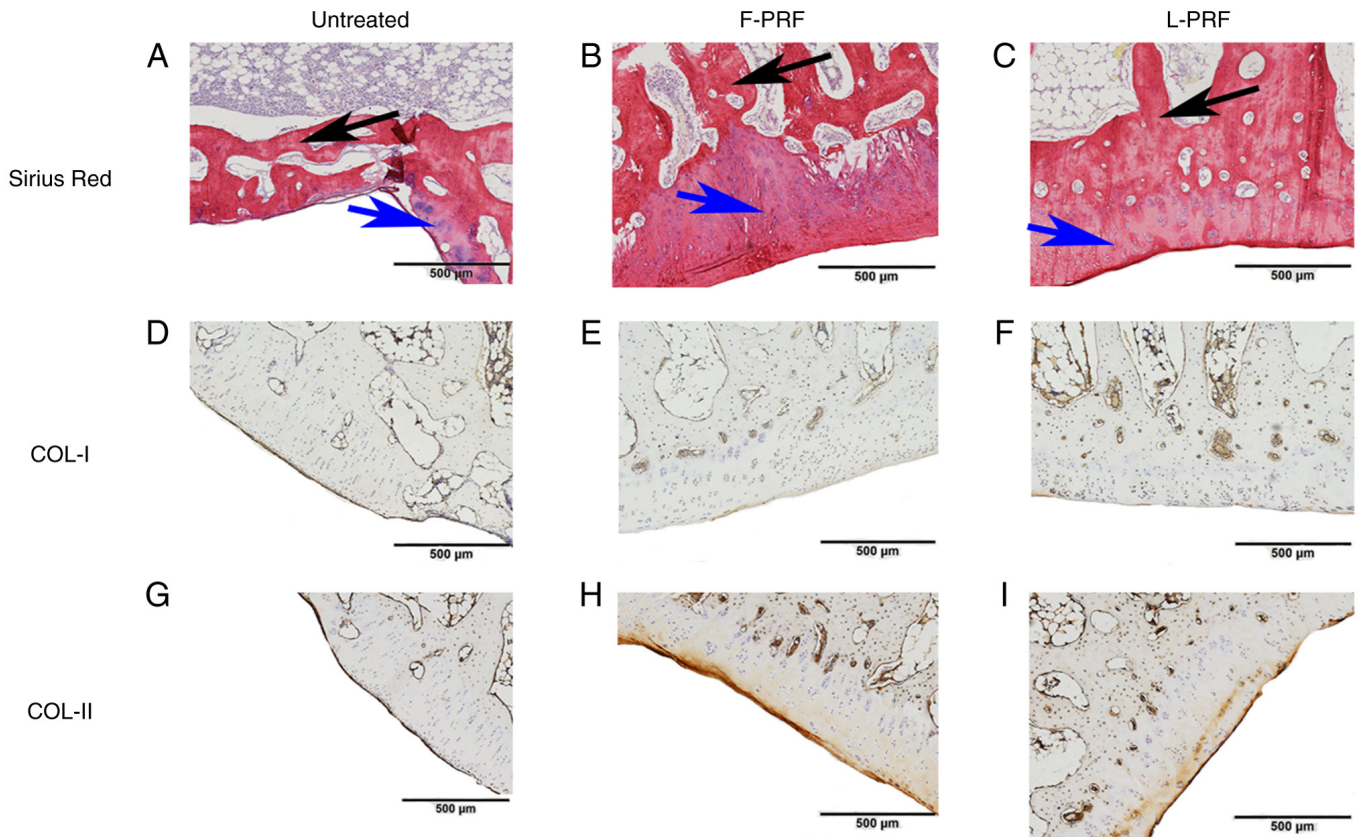
Figure 5. Sirius red staining and immunostaining at 16 weeks postoperatively. (A) Sirius red staining showed different kinds of regenerated collagen in all three groups. In detail, there were large masses of regenerated cartilage matrix (blue arrow) and bone matrix (black arrow) in the (B) F-PRF and (C) L-PRF groups. However, only a small amount of newly regenerated cartilage matrix (blue arrow) was observed in the (A) Untreated group. (D-F) COL-I immunostaining. (G-I) COL-II immunostaining. COL-I, collagen type I; COL-II, collagen type II; PRF, platelet-rich fibrin; L-PRF, lyophilized PRF; F-PRF, free PRF.

newly formed cartilage tissues in the PRF-treated groups (Fig. 5H and I). Moreover, COL-II staining was weak in the untreated group because the amount of newly formed cartilage was minimal (Fig. 5G). Furthermore, the mean density of COL-I and COL-II in the PRF-treated groups was also similar to that in the positive control. Finally, the quantitative analysis of the immunohistochemical COL-I and COL-II staining also provided similar results; that is, there was no significant difference between the F-PRF and L-PRF groups, but both of them had significantly higher values than those in the untreated group (Fig. S3).

Discussion

The present study demonstrated that full-thickness osteochondral defects 5 mm in diameter and 4 mm in depth could be successfully reconstructed by implanting F-PRF or L-PRF scaffolds, without the need for additional cell seeding, and the simultaneous reconstruction of avascular articular cartilage and well-regenerated subchondral bone was proven through macroscopic observations, micro-CT scanning and histological examinations. Compared with several commonly reported approaches used for the repair and regeneration of osteochondral defects, the present method possesses the following advantages: First, F-PRF and L-PRF are derived wholly from autologous blood, they are convenient and versatile, have a high ratio of quality to price. For example, for bone defects after

dental implant and apical cyst curettage in the dental clinic, if GBR is performed at the same time, the cost of bone powder, collagen membrane and membrane nail will be a large amount of cost. However, if PRF is used, only a small amount of the cost of autologous blood centrifugation is required. Relatively speaking, it reduces economic burden for patients.) and lack the drawback of donor morbidity (14). Second, autologous F-PRF and L-PRF, as rich sources of growth factors and bioactive scaffolds, provide good biocompatibility and no risk of immunological rejection. Third, this method does not require additional cell transplantation or an exogenous scaffold for cell transportation; therefore, it can avoid the shortcomings of implanting such scaffolds or cells (7). Finally, transplanted F-PRF or L-PRF scaffolds retained the blood effused from subchondral bone marrow, which contained a mass of BMSCs, within the osteochondral defects, thus initiating the process of wound healing and improving the remodeling of newly formed tissues (23).

Due to the gradual release of large amounts of growth factors that can accelerate tissue regeneration and remodeling during the biodegradation of PRF, this has been broadly applied in tissue engineering and regenerative medicine (24-27). However, one limitation of the PRF application is that it has to be used immediately, commonly within 10 min after preparation. In a previous study performed by the present authors, L-PRF was processed and prepared by vacuum freeze-drying F-PRF and the effect of these two PRFs on the osteogenicity

of BMSCs was compared *in vitro* and *in vivo* (16). The results of the present study indicated that the lyophilization of F-PRF had a slight effect on the microstructure of the PRF, which was verified through H&E staining and SEM examination. L-PRF was composed of abundant compactly arranged fibers and could release growth factors. SEM observations showed that BMSCs possessed good attachment on the surface of both F-PRF and L-PRF (Fig. S4). In addition, L-PRF markedly increased the osteogenicity and proliferation of BMSCs in a dose-dependent manner *in vitro* and stimulated the osteogenicity of osteoblastic BMSC sheets *in vivo* (Fig. S5) (16). The numerous 3-D network microstructures of L-PRF could stimulate cell migration and tissue bonding (28). Furthermore, because the contact surface area of L-PRF was increased, lyophilization not only facilitated cell proliferation and mineralization by increasing the pore size of L-PRF but also increased the degradation rate of L-PRF, which was verified to be faster than that of F-PRF (29,30). In addition, F-PRF and L-PRF could recruit stem cells to targeted sites and then initiate the tissue repair process by stimulating the rapid proliferation and differentiation of BMSCs (11,26). These results suggest that L-PRF can be considered an emerging biomaterial that adequately supplies the persistent discharge of cytokines and growth factors that are crucial for tissue repair and regeneration (31,32).

Successful wound repair in various kinds of adult tissues relies strongly on the process of repair mediated by a stable blood clot that can release a mass of cues attracted by hemostasis and trigger the recruitment and migration of cells (9,33). Therefore, an essential and stable blood clot in defects of the articular knee joint could stimulate cartilage repair and subchondral bone reconstruction by offering a stable microenvironment for surrounding stem cell recruitment and migration and tissue regeneration (23,34). On the other hand, osteochondral defects on the femoral condyle joint provided an opening and suitable microenvironment for recruiting cells from the surrounding joint cavity, synovium, and, most importantly, from the subchondral bone marrow (7,35). During surgery, PRF fragments placed in the defect site promptly transformed into soft matrices after absorbing bone marrow blood. In addition, because of the 3-D fibrous network and bioactive cytokines or growth factors that appeared in the L-PRF and F-PRF scaffolds, PRF scaffolds can recruit progenitor or stem cells from the subchondral bone marrow or surrounding synovium and stimulate them to transfer through channels among PRF fragments, which also stimulates the recruited and migrated progenitor or stem cells to undergo proliferation and differentiation (36,37). The upper part of the defect in the joint surface was enclosed by surrounding articular cartilage and the recruited cells were influenced by the biological cues from the cartilage and joint fluid, which formed a chondrogenic environment (6,7,38). By contrast, the lower part of the osteochondral defects was directly connected with the bone marrow cavity and enclosed by the surrounding subchondral bone, which has been proven to be strongly osteogenic. BMSCs undergo endochondral ossification with the induction of osteogenic medium and chondrogenesis occurs during this process and before ossification (39). Therefore, environmental factors play a dominant role in the reconstruction of osteochondral defects, including the engineering of

cartilage and subchondral bone (40). Furthermore, histological results showed that a decreased inflammation occurred, which confirmed the excellent biocompatibility of autologous F-PRF and L-PRF scaffolds. Concerning implantation, blood clots are mixed with transplanted PRF fragments, which provide an opening microenvironment. Such a microenvironment enables migrated cells to experience a low oxygen level, which is considered to promote chondrogenesis in the upper part of osteochondral defects (41,42). Moreover, the natural structure of the load-bearing femoral condyle poses the risk of PRF scaffold displacement and remodeling. The purpose of the present study was to discuss the effect of L-PRF scaffolds on the reconstruction of osteochondral defects. Hence, the trochlear groove was selected as the experimental model of defects in rabbits.

Mechanical testing is more frequently used for examining the mechanical properties of the articular cartilage (7). However, F-PRF or L-PRF fragments used in this experiment are small in thickness, which could not meet the requirements for compressive tests. In addition, the trochlear groove was chosen as the defect model as the present study is a preliminary attempt to test the osteochondral reconstruction using L-PRF fragments. Load-bearing femoral condyle model inevitably increases the risk of scaffold collapse and displacement, mainly owing to their weak mechanical strength. The present study aimed to investigate the cell-recruiting and cartilage-repairing effects of F-PRF or L-PRF fragments. Although only one treatment displayed good satisfactory effect in the present rabbit model, multiple treatments may be required on large animals like dogs or pigs, which needs further study.

The newly formed cartilage tissue failed to achieve complete regeneration because the zonal hierarchical structure of the native osteochondral tissue could not be completely reconstructed (23). Therefore, the present results indicated that the PRF scaffolds elicited tissue regeneration, which could be regarded as cartilage replacement. Because an osteochondral defect 5 mm in diameter and 4 mm in depth was produced in knee joints *in vivo*, the regenerated tissue was damaged when the newly reconstructed cartilage and subchondral bone were harvested; therefore, the compressive strength assay was not performed. In the future, a larger defect in larger model animals will be created (such as miniature pigs and goats) to test the compressive strength of the reconstructed cartilage tissue.

The present study demonstrated that autologous L-PRF prepared by freeze-drying F-PRF significantly improved the reconstruction of osteochondral defects in the knee joint of rabbits, thus offering a novel bioscaffold for the simultaneous regeneration of subchondral bone and articular cartilage without cell transplantation.

Availability of data and materials

The datasets used and/or analyzed during the current study are available from the corresponding author on reasonable request.

Authors' contributions

JWS, LH and ZFW conceived and designed the study. JWS, LH and CDL carried out *in vitro* and *in vivo* studies, participated in the sequence alignment and drafted the manuscript. JLM, XL and SHS carried out the *in vitro* and *in vivo* studies. SHS and ZFW confirm the authenticity of all the raw data and performed the statistical analysis. All authors read and approved the final version of the manuscript.

Ethics approval and consent to participate

The animal experiments were reviewed and approved by the Institutional Animal Care and Use Committee of the General Hospital of Southern Theater of PLA (Guangzhou, China; approval no. 2019010402).

Patient consent for publication

Not applicable.

Competing interests

The authors declare that they have no competing interests.

References

1. Deng C, Chang J and Wu C: Bioactive scaffolds for osteochondral regeneration. J Orthop Translat 17: 15-25, 2018.
2. Xue J, Feng B, Zheng R, Lu Y, Zhou G, Liu W, Cao Y, Zhang Y and Zhang WJ: Engineering ear-shaped cartilage using electrospun fibrous membranes of gelatin/polycaprolactone. Biomaterials 34: 2624-2631, 2013.
3. Huey DJ, Hu JC and Athanasiou KA: Unlike bone, cartilage regeneration remains elusive. Science 338: 917-921, 2012.
4. Brittberg M, Lindahl A, Nilsson A, Ohlsson C, Isaksson O and Peterson L: Treatment of deep cartilage defects in the knee with autologous chondrocyte transplantation. N Engl J Med 331: 889-895, 1994.
5. Nooeaid P, Salih V, Beier JP and Boccaccini AR: Osteochondral tissue engineering: Scaffolds, stem cells and applications. J Cell Mol Med 16: 2247-2270, 2012.
6. Mendelson A, Frank E, Allred C, Jones E, Chen M, Zhao W and Mao JJ: Chondrogenesis by chemotactic homing of synovium, bone marrow, and adipose stem cells in vitro. FASEB J 25: 3496-3504, 2011.
7. Wang Z, Li Z, Li Z, Wu B, Liu Y and Wu W: Cartilaginous extracellular matrix derived from decellularized chondrocyte sheets for the reconstruction of osteochondral defects in rabbits. Acta Biomater 81: 129-145, 2018.
8. Lee CH, Cook JL, Mendelson A, Moioli EK, Yao H and Mao JJ: Regeneration of the articular surface of the rabbit synovial joint by cell homing: A proof of concept study. Lancet 376: 440-448, 2010.
9. Zlotnick HM, Locke RC, Stoeckl BD, Patel JM, Gupta S, Browne KD, Koh J, Carey JL and Mauck RL: Marked differences in local bone remodelling in response to different marrow stimulation techniques in a large animal. Eur Cell Mater 41: 546-557, 2021.
10. Park MS, Kim YH, Jung Y, Kim SH, Park JC, Yoon DS, Kim SH and Lee JW: In situ recruitment of human bone marrow-derived mesenchymal stem cells using chemokines for articular cartilage regeneration. Cell Transplant 24: 1067-1083, 2015.
11. Kazemi D, Fakhrjou A, Dizaji VM and Alishahi MK: Effect of autologous platelet rich fibrin on the healing of experimental articular cartilage defects of the knee in an animal model. Biomed Res Int 2014: 486436, 2014.
12. Dohan DM, Choukroun J, Diss A, Dohan SL, Dohan AJ, Mouhyi J and Gogly B: Platelet-rich fibrin (PRF): A second-generation platelet concentrate. Part I: Technological concepts and evolution. Oral Surg Oral Med Oral Pathol Oral Radiol Endod 101: e37-e44, 2006.
13. Serra CI, Soler C, Carrillo JM, Sopena JJ, Redondo JI and Cugat R: Effect of autologous platelet-rich plasma on the repair of full-thickness articular defects in rabbits. Knee Surg Sports Traumatol Arthrosc 21: 1730-1736, 2013.
14. Wang Z, Weng Y, Lu S, Zong C, Qiu J, Liu Y and Liu B: Osteoblastic mesenchymal stem cell sheet combined with Choukroun platelet-rich fibrin induces bone formation at an ectopic site. J Biomed Mater Res B Appl Biomater 103: 1204-1216, 2015.
15. Wang Z, Hu H, Li Z, Weng Y, Dai T, Zong C, Liu Y and Liu B: Sheet of osteoblastic cells combined with platelet-rich fibrin improves the formation of bone in critical-size calvarial defects in rabbits. Br J Oral Maxillofac Surg 54: 316-321, 2016.
16. Wang Z, Han L, Sun T, Wang W, Li X and Wu B: Preparation and effect of lyophilized platelet-rich fibrin on the osteogenic potential of bone marrow mesenchymal stem cells in vitro and in vivo. Heliyon 5: e02739, 2019.
17. Lei X, Yang Y, Shan G, Pan Y and Cheng B: Preparation of ADM/PRP freeze-dried dressing and effect of mice full-thickness skin defect model. Biomed Mater 14: 035004, 2019.
18. Chumroenphat T, Somboonwatthanakul I, Saensouk S and Siriamornpun S: Changes in curcuminoids and chemical components of turmeric (Curcuma longa L.) under freeze-drying and low-temperature drying methods. Food Chem 339: 128121, 2021. Haugh MG, Murphy CM and O'Brien FJ: Novel freeze-drying methods to produce a range of collagen-glycosaminoglycan scaffolds with tailored mean pore sizes. Tissue Eng Part C Methods 16: 887-894, 2010.
19. Shi L, Li R, Wei S, Zhou M, Li L, Lin F, Li Y, Guo Z, Zhang W, Chen M and Shan G: Effects of a protective agent on freeze-dried platelet-rich plasma. Blood Coagul Fibrinolysis 30: 58-65, 2019.
20. Ba R, Wei J, Li M, Cheng X, Zhao Y and Wu W: Cell-bricks based injectable niche guided persistent ectopic chondrogenesis of bone marrow-derived mesenchymal stem cells and enabled nasal augmentation. Stem Cell Res Ther 6: 16, 2015.
21. van den Borne MP, Raijmakers NJ, Vanlauwe J, Victor J, de Jong SN, Bellemans J and Saris DB; International Cartilage Repair Society: International cartilage repair society (ICRS) and oswestry macroscopic cartilage evaluation scores validated for use in autologous chondrocyte implantation (ACI) and microfracture. Osteoarthritis Cartilage 15: 1397-1402, 2007.
22. Mainil-Varlet P, Van Damme B, Nesic D, Knutsen G, Kandel R and Roberts S: A new histology scoring system for the assessment of the quality of human cartilage repair: ICRS II. Am J Sports Med 38: 880-890, 2010.
23. Wang Z, Han L, Sun T, Ma J, Sun S, Ma L and Wu B: Extracellular matrix derived from allogenic decellularized bone marrow mesenchymal stem cell sheets for the reconstruction of osteochondral defects in rabbits. Acta Biomater 118: 54-68, 2020.
24. Temmerman A, Cleeren GJ, Castro AB, Teughels W and Quirynen M: L-PRF for increasing the width of keratinized mucosa around implants: A split-mouth, randomized, controlled pilot clinical trial. J Periodontal Res 53: 793-800, 2018.
25. Sameera S, Nagasri M, Aravind Kumar P, Indeevar P, Raviraj K and Musalaiah SVVS: Comparison of two surgical techniques in the treatment of multiple gingival recessions sandwiched with a combination of A-PRF and L-PRF. Saudi Dent J 30: 183-189, 2018.
26. Beitzel K, McCarthy MB, Cote MP, Russell RP, Apostolakos J, Ramos DM, Kumbar SG, Imhoff AB, Arciero RA and Mazzocca AD: Properties of biologic scaffolds and their response to mesenchymal stem cells. Arthroscopy 30: 289-298, 2014.
27. Dohan DM, Choukroun J, Diss A, Dohan SL, Dohan AJ, Mouhyi J and Gogly B: Platelet-rich fibrin (PRF): A second-generation platelet concentrate. Part III: Leucocyte activation: a new feature for platelet concentrates? Oral Surg Oral Med Oral Pathol Oral Radiol Endod 101: e51-e55, 2006.

28. Ma L, Wang X, Zhao N, Zhu Y, Qiu Z, Li Q, Zhou Y, Lin Z, Li X, Zeng X, *et al*: Integrating 3D printing and biomimetic mineralization for personalized enhanced osteogenesis, angiogenesis, and osteointegration. ACS Appl Mater Interfaces 10: 42146-42154, 2018.

29. Isobe K, Watanebe T, Kawabata H, Kitamura Y, Okudera T, Okudera H, Uematsu K, Okuda K, Nakata K, Tanaka T and Kawase T: Mechanical and degradation properties of advanced platelet-rich fibrin (A-PRF), concentrated growth factors (CGF), and platelet-poor plasma-derived fibrin (PPTF). Int J Implant Dent 3: 17, 2017.

30. Pichotano EC, de Molon RS, de Souza RV, Austin RS, Marcantonio E and Zandim-Barcelos DL: Evaluation of L-PRF combined with deproteinized bovine bone mineral for early implant placement after maxillary sinus augmentation: A randomized clinical trial. Clin Implant Dent Relat Res 21: 253-262, 2019.

31. Lundquist R, Dziegiel MH and Agren MS: Bioactivity and stability of endogenous fibrogenic factors in platelet-rich fibrin. Wound Repair Regen 16: 356-363, 2008.

32. Dohan Ehrenfest DM, Del Corso M, Diss A, Mouhyi J and Charrier JB: Three-dimensional architecture and cell composition of a Choukroun's platelet-rich fibrin clot and membrane. J Periodontol 81: 546-555, 2010.

33. White JG: Platelet secretion during clot retraction. Platelets 11: 331-343, 2000.

34. Mao Z, Bi X, Wu C, Zheng Y, Shu X, Wu S, Guan J and Ritchie RO: A cell-free silk fibroin biomaterial strategy promotes in situ cartilage regeneration via programmed releases of bioactive molecules. Adv Healthc Mater 12: e2201588, 2023.

35. Ravindran S, Kotecha M, Huang CC, Ye A, Pothirajan P, Yin Z, Magin R and George A: Biological and MRI characterization of biomimetic ECM scaffolds for cartilage tissue regeneration. Biomaterials 71: 58-70, 2015.

36. Crapo PM, Gilbert TW and Badylak SF: An overview of tissue and whole organ decellularization processes. Biomaterials 32: 3233-3243, 2011.

37. Cortiella J, Niles J, Cantu A, Brettler A, Pham A, Vargas G, Winston S, Wang J, Walls S and Nichols JE: Influence of acellular natural lung matrix on murine embryonic stem cell differentiation and tissue formation. Tissue Eng Part A 16: 2565-2580, 2010.

38. Li Z, Ba R, Wang Z, Wei J, Zhao Y and Wu W: Angiogenic potential of human bone marrow-derived mesenchymal stem cells in chondrocyte brick-enriched constructs promoted stable regeneration of craniofacial cartilage. Stem Cells Transl Med 6: 601-612, 2017.

39. Li J, Kang F, Gong X, Bai Y, Dai J, Zhao C, Dou C, Cao Z, Liang M, Dong R, *et al*: Ceria nanoparticles enhance endochondral ossification-based critical-sized bone defect regeneration by promoting the hypertrophic differentiation of BMSCs via DHX15 activation. FASEB J 33: 6378-6389, 2019.

40. Gaut C and Sugaya K: Critical review on the physical and mechanical factors involved in tissue engineering of cartilage. Regen Med 10: 665-679, 2015.

41. Nukavarapu SP and Dorcemus DL: Osteochondral tissue engineering: current strategies and challenges. Biotechnol Adv 31: 706-721, 2013.

42. Brown BN and Badylak SF: Extracellular matrix as an inductive scaffold for functional tissue reconstruction. Transl Res 163: 268-285, 2014.